Chemical Engineering Journal 421 (2021) 129825

Contents lists available at ScienceDirect

Chemical Engineering Journal

journal homepage: www.elsevier.com/locate/cej

Sulfur-doped triazine-conjugated microporous polymers for achieving the robust visible-light-driven hydrogen evolution

Ahmed M. Elewa [a,b], Ahmed F.M. EL-Mahdy [c,*], Mohamed Hammad Elsayed [a], Mohamed Gamal Mohamed [c], Shiao-Wei Kuo [c,d,*], Ho-Hsiu Chou [a,*]

[a] Department of Chemical Engineering, National Tsing Hua University, No. 101, Sec. 2, Kuang-Fu Rd., Hsinchu 30013, Taiwan
[b] Nuclear Chemistry Department, Hot Laboratories Center, Atomic Energy Authority, P.O. Box 13759, Inshas, Cairo, Egypt
[c] Department of Materials and Optoelectronic Science, National Sun Yat-Sen University, Kaohsiung 80424, Taiwan
[d] Department of Medicinal and Applied Chemistry, Kaohsiung Medical University, Kaohsiung 807, Taiwan

ARTICLE INFO

Keywords:
Conjugated microporous polymers (CMPs)
Triazine-based CMPs
Sulfur doping
Visible-light
Hydrogen evolution

ABSTRACT

Conjugated microporous polymers (CMPs) have emerged in recent years as prospective materials for photocatalytic hydrogen production. The most common synthesis method for triazine is ionothermal synthesis at high temperatures (>350 °C), which also requires a large amount of $ZnCl_2$, in which CF_3SO_3H-catalyzed method was invented to synthesize triphenyl triazine at room temperature. Herein, we reported the synthesis and characterization of two triazine-based conjugated micropores polymers photocatalysts at low temperature via polymerization of triphenyl triazine (TPT) with TPT and pyrene (Py). The TPT-based CMPs show excellent photocatalytic performance and a hydrogen evolution rate of 108.1 and 116.5 μmol h^{-1} under visible light for Py-TPT-CMP and TPT-TPT-CMP, respectively, but with low photocatalytic stability. In general, organic polymers add a small amount of platinum to efficiently produce H_2 with high photocatalyst stability. To provide a new opportunity to overcome the low stability, a sulfur doping method using readily available sulfur (S8) has been proposed which was used here for the first time to achieve a highly photocatalyst stability development without the use of noble metals. The as-synthesized polymers after sulfur doped exhibit an enhanced photocatalytic stability which can keep the hydrogen production for a long period of time without loss in the photocatalytic efficiency. Furthermore, our triazine-based CMP materials have interest apparent quantum yield (AQY) values particularly for Py-TPT-CMP and TPT-TPT-CMP which exhibit AQY of 41.9 and 32.38%, respectively at 420 nm, these values are compatible with the highest AQY of organic photocatalysts up to date. This study makes a significant contribution forward for photocatalysis with polymers because it provides excellent HERs and AQYs for the sulfur-doped triazine-based CMPs with high thermal, chemical, and photo stabilities. As well as, this work could give researchers in the field a different opinion on the effect of sulfur-doping.

1. Introduction

Photocatalytic production of hydrogen from water using solar energy has been thoroughly studied, as it allows the efficient development of renewable fuels from plentiful resources [1,2]. So far, most photocatalysts have been inorganic materials [3–10], but organic photocatalysts have attracted increasing attention [11–14]. Where, organic photocatalysts have several advantages such as low-cost, easy to process, free of toxic metals, easily band gap tunable, structural diversity, and functional flexibility [15]. Graphite carbon nitride (g-C_3N_4), has been shown to be promising material for H_2 production due to their facile synthesis, high physicochemical stability, and attractive electronic band structure [16–23]. However, the photocatalytic efficiency of pure g-C_3N_4 is still limited due to several barriers, such as low surface area without generating toned pores, harsh synthesis condition such as the synthesis is carried out at high temperature > 500 °C, and high electron-hole recombination rate [24–26]. In recent years, a number of conjugated organic photocatalysts have now been reported to exhibit photocatalytic hydrogen production from water using visible light, including oligomers, linear polymers [14,27], polymer dot [28,29], hydrophilic polymers [30,31], porous heptazine based polymers [32,33], metal organic frameworks (MOFs) [34,35], and covalent organic frameworks

* Corresponding authors.
E-mail addresses: ahmedelmahdy@mail.nsysu.edu.tw (A.F.M. EL-Mahdy), kuosw@faculty.nsysu.edu.tw (S.-W. Kuo), hhchou@mx.nthu.edu.tw (H.-H. Chou).

https://doi.org/10.1016/j.cej.2021.129825
Received 7 February 2021; Received in revised form 7 April 2021; Accepted 11 April 2021
Available online 15 April 2021

(COFs) [36–39]. Recent studies have revealed that conjugated microporous polymers (CMPs) are promising for efficient photocatalysts for hydrogen evolution due to their high surface area, diverse synthetic strategies, reasonable carrier mobility, and controllable bandgap, which allow their chemical structure and electronic property to be finely tailored [40,41]. It was found that triphenyl triazine with nitrogen free electron pair is an efficient building block for the construction of CMP photocatalysts to improve photocatalytic hydrogen evolution due to the hydrophilic nature of nitrogen atoms so can act as the active site for an interface redox reaction. However, triazine-based polymers or covalent triazine frameworks (CTFs) are similar to g-C_3N_4 in terms of their high nitrogen content and their synthesis which often, includes ionothermal method in molten salt mixtures at high temperatures above 350 °C, which also requires a large amount of $ZnCl_2$ to act as a catalyst and reaction medium. CTFs for photocatalytic H_2 evolution were prepared at 400 °C [42], and also obtained for water oxidation and proton reduction by a microwave synthesis at 200 °C [43]. Very recently, Voort and co-workers reported synthesized CTF-1 for oxygen reduction and hydrogen evolution were prepared at 500 °C [44]. Moreover, high reaction temperatures cause partial carbonization of the structure, consume a large amount of energy, and inhibit all but the most stable building blocks, thus limiting the range of expansion and compositional diversity. To further overcome these limitations, many research groups have interested in using an effective low-temperature polycondensation reaction to synthesize triazine-based conjugated micropores polymers (TPT-based CMPs) photocatalyst at mild conditions, which allows various building blocks to be used. Our group developed TPT-based CMPs at low temperature, where trifluoromethanesulfonic acid (CF_3SO_3H) catalyzed method was used to synthesize triphenyl triazine at room temperature, by which TPT-based CMPs could be obtained and their tunable bandgap structures could be achieved. Through this method, TPT-based CMPs can be designed from versatile building blocks and demonstrated high potential in photocatalytic applications. In order to achieve excellent photocatalytic performance, it is important to select appropriate building blocks in polymer structures. Therefore, several structures have been used in the synthesis of triazine-based CMPs. Some building blocks such as pyrene (Py) and triphenyl triazine (TPT) have been widely explored in the synthesis of porous polymers due to their high surface area, reasonable carrier mobility, and high thermal stability. Even though, Py unit has already been reported in the synthesis of several porous materials [45–48], it has not yet been used in the synthesis of TPT-based CMPs. Triphenyl triazine block (TPT) was reported to synthesize CTFs using the CF_3SO_3H catalytic method. Cooper and co-workers reported synthesized of CTF-2 (TPT-TPT-CMP) as an efficient photocatalyst for hydrogen evolution by CF_3SO_3H catalysis from nitriles at 80 °C with hydrogen evolution rate (HER) about 6.6 μmol h^{-1} using triethanolamine (TEOA) and a Pt co-catalyst [26]. Also, Wang and co-workers reported synthesized of CTF-2 (TPT-TPT-CMP) photocatalyst for hydrogen and oxygen evolution with photocatalytic HER up to 25 μmol h^{-1} using TEOA and a Pt co-catalyst was synthesized using CF_3SO_3H catalysis from nitriles at 100 °C [49]. Here, we synthesized the TPT using CF_3SO_3H at room temperature to synthesize TPT-TPT-CMP for photocatalytic H_2 evolution. Notably, we observed the sacrificial electron donor (SED) is highly affected the photocatalytic efficiency of TPT-TPT-CMP. TPT-TPT-CMP was presented a low HER of about 10.78 μmol h^{-1} when using the same conditions as above papers. Whereas, we can further improve the HER of TPT-TPT-CMP up to116.5 μmol h^{-1} by introducing the triethylamine (TEA) as SED. However, even though the efficiency of the TPT-TPT-CMP can be enhanced by selecting the proper SED, its photocatalytic stability was poor.

To efficiently produce H_2 with high photostability of catalyst, generally, organic polymers are added a small amount of platinum (Pt) and a sacrificial electron donor, which can attract the photogenerated electrons, and donates its electrons to the photogenerated holes to protect the polymers from degradation, respectively [50,51]. Although the incorporation of Pt can efficiently enhance the photocatalytic reaction, the development of photocatalysts with high photocatalytic efficiency as well as high photocatalytic stability without Pt is still a promising design strategy [52]. Because the Pt cocatalysts are too scarce and high-cost to be used for large-scale energy production [53], it is crucial to seek an alternative to Pt cocatalysts that can match enhancement the photostability of a photocatalyst. Generally, chemical doping is an effective way to modify the electronic structures and surface properties of semiconductors [54–59]. The element sulfur is known as an elusive dopant which can modulate both the optical absorption properties and the electronic structure of nitrogen-based organic semiconducting photocatalytic materials [54,60,61]. Several papers reported the doping of sulfur can enhance the efficiency of photocatalytic hydrogen evolution due to the enhanced light absorbance and efficient charge transfer [54,56,62,63]. Although, these studies have shown that sulfur-doped g-C_3N_4 or CTFs can effectively improve the photocatalytic efficiency of hydrogen evolution. However, in their work, the CTF before sulfur-doping already showed good stability, there was no difference before and after sulfur-doping. Therefore, it cannot tell the effect of the sulfur-doping for improve the stability. However, to the best of our knowledge, there are no reports on enhancing the photocatalytic stability of hydrogen evolution for TPT-based CMPs using sulfur doping.

In this work, for the first time, we demonstrated that actually the sulfur-doped TPT-based CMP was decreased the HER efficiency compare to the one without sulfur-doping (but still compatible to the other works, see Table S7), while the stability of photocatalytic hydrogen evolution can be enhanced. Additionally, as it is known for a real application, the total amount of H_2 produced is more important than the rate of H_2 production.

2. Experimental section

2.1. Material

All chemicals utilized for conducting the experimental work of this investigation were analytical grade and used without further purification. Pyrene (98%) and Tetrakis(triphenylphosphine)palladium(0) (99%) were obtained from Acros, 1,1′-Bis(diphenylphosphino)ferrocene]dichloropalladium(II), Bis(pinacolato)diboron 99%, Potassium carbonate, Sublimed sulfur, Bromine (99.99%), triethylamine (TEA), ascorbic acid, and triethanolamine (TEOA) were purchased from Sigma-Aldrich. Trifluoromethanesulfonic Acid (F_3CSO_3H) and 4-bromobenzonitrile was obtained from Alfa Aesar. Dimethylformamide (DMF), 1,4-Dioxane, Nitrobenzene, and Chloroform were purchased from J. T. Baker. Methanol was purchased from Kelong Chemistry Reagent Co. Ltd. (Chengdu, China). Deionized water was applied in all the experiments.

2.2. Synthetic procedures

2.2.1. Synthesis of 2,4,6-tris(4-bromophenyl)-1,3,5-triazine (TPT-3Br)

Prepared as described in the literature, with minor modifications [64,65]. In a 100 mL two neck-bottle under nitrogen atmosphere, a solution of 4-bromobenzonitrile (1.5 g, 8.24 mmol) in dry chloroform (20 mL) was cooled to 0 °C and then trifluoromethanesulfonic acid (4 mL, 0.045 mmol) was drop wisely added. The reaction mixture was stirred for 30 min at 0 °C and then warmed to room temperature. After stirring for an additional 20 h at room temperature, the reaction solution was poured into ice-water (50 mL). The aqueous solution was neutralized by sodium carbonate (Na_2CO_3). The formed precipitate was collected by filtration and dried under vacuum overnight to yield 2,4,6-tris(4-bromophenyl)-1,3,5-triazine as a white solid. FT-IR (powder): 1578, 1518, 1400, 1372, 1173, 1069, 1011, 843, 806, 498 cm^{-1}. ^1H NMR ($CDCl_3$, 25 °C, 500 MHz): 8.60 (d, $J = 8.5$ Hz, 6H), 7.70 (d, $J = 8.5$ Hz, 6H). ^{13}C NMR ($CDCl_3$, 25 °C, 125 MHz): 171.22, 134.91, 132.01, 130.48, 127.88.

2.2.2. Synthesis of Py-TPT-CMP

A mixture of 1,3,6,8-tetrabromopyrene (100 mg, 0.19 mmol), 2,4,6-tris(4-(4,5-dimethyl-1,3,2-dioxaborolan-2-yl)phenyl)-1,3,5-triazine (177 mg, 0.26 mmol), potassium carbonate (356 mg, 2.6 mmol),tetrakis (triphenylphosphine)palladium(0) (30 mg, 0.026 mmol) were put in a Pyrex tube (25 mL) and then DMF (10 mL) and H_2O (2 mL) were added. The reaction mixture was degassed by three freeze–pump–thaw cycles and purged with N_2 to remove the oxygen from the system. The tube was then heated at 150 °C for 3 days. After cooling to 25 °C, the reaction mixture was collected by centrifugation and washed with acetone (3 times) and THF (3 times) until the solution became colorless and the solid product was dried at 100 °C for overnight under vacuum to give Py-TPT-CMP as green solid, yield (75%).

2.2.3. Synthesis of TPT-TPT-CMP

A mixture of 2,4,6-tris(4-bromophenyl)-1,3,5-triazine (150 mg, 0.27 mmol), 2,4,6-tris(4-(4,5-dimethyl-1,3,2-dioxaborolan-2-yl)phenyl)-1,3,5-triazine (189 mg, 0.27 mmol), potassium carbonate (379 mg, 2.7 mmol),tetrakis(triphenylphosphine)palladium(0) (33 mg, 0.027 mmol) were put in a Pyrex tube (25 mL) and then DMF (10 mL) and H_2O (2 mL) were added. The reaction mixture was degassed by three freeze–pump–thaw cycles and purged with N_2 to remove the oxygen from the system. The tube was then heated at 150 °C for 3 days. After cooling to 25 °C, the reaction mixture was collected by centrifugation and washed with acetone (3 times) and THF (3 times) until the solution became colorless and the solid product was dried at 100 °C for overnight under vacuum to give TPT-TPT-CMP as gray solid, yield (70%).

2.2.4. Synthesis of Py-TPT-CMP-S_x

Py-TPT-CMP (100 mg) was mixed with 10 wt% (10 mg) or 20 wt% (20 mg) of sublimed sulfur and then grinded well in an agate. The mixed powder was transferred into a quartz crucible and then heated at 300 °C for 5 h with a ramping rate of 5 °C per min under nitrogen atmosphere. After cooling to 25 °C, the solid product was washed with methanol and collected by filtration. The final product was dried at 60 °C for overnight to yield Py-TPT-CMP-S_{10} or Py-TPT-CMP-S_{20}.

2.2.5. Synthesis of TPT-TPT-CMP-S_x

TPT-TPT-CMP (100 mg) was mixed with 10 wt% (10 mg) or 20 wt% (20 mg) of sublimed sulfur and then grinded well in an agate. The mixed powder was transferred into a quartz crucible and then heated at 300 °C for 5 h with a ramping rate of 5 °C per min under nitrogen atmosphere. After cooling to 25 °C, the solid product was washed with methanol and collected by filtration. The final product was dried at 60 °C for overnight to yield TPT-TPT-CMP-S_{10} or TPT-TPT-CMP-S_{20}.

2.3. Materials characterizations

^1H and ^{13}C NMR spectroscopy were recorded using an INOVA 500 instrument with DMSO-d_6 and $CDCl_3$ as solvents and tetramethylsilane (TMS) as the external standard. Chemical shifts are provided in parts per million (ppm). The energy levels of the HOMOs were measured using a photoelectron spectrometer (model AC-2). The energy levels of the LUMOs were calculated by subtracting the E_g from the HOMO energy levels. The X-ray powder diffraction (XRD) pattern was recorded by using an X' Pert Pro diffractometer equipped with Cu Kα radiation. The scanning rate is 4° min^{-1}. The BET surface areas and porosimetry measurements of the prepared samples (ca. 20–100 mg) were performed using a Micromeritics ASAP 2020 Surface Area and Porosity analyzer. Nitrogen isotherms were generated through incremental exposure to ultrahigh-purity N_2 (up to ca. 1 atm) in a liquid N_2 (77 K) bath. The thermogravimetric analyses (TGA) was performed using a TA Q-50 analyzer under a flow of N_2. The samples were sealed in a Pt cell and heated from 40 to 800 °C at a heating rate of 20 °C min^{-1} under N_2 at a flow rate of 50 mL min^{-1}. The BET surface areas and porosimetry measurements of the prepared samples (ca. 20–100 mg) were performed using a Micromeritics ASAP 2020 Surface Area and Porosity analyzer. Nitrogen isotherms were generated through incremental exposure to ultrahigh-purity N_2 (up to ca. 1 atm) in a liquid N_2 (77 K) bath. A Hitachi U-3300 spectrophotometer was used to obtain the UV–visible absorption spectra. A BRUKE Tensor-27 spectrometer was used for obtaining the Fourier transformation infrared (FTIR) spectroscopy, with a resolution of 4 cm^{-1}. The photoluminescence (PL) spectra were recorded using a Hitachi F-7000 spectrophotometer, with an excitation wavelength of 350 nm, at room temperature. Time resolved transient spectra of the polymer photocatalysts were measured on a spectrometer (FLS980, Edinburgh Instruments) with a gated photomultiplier tube. TEM was performed using a JEOL-2100 scanning electron microscope, operated at 200 kV. FE-SEM was conducted using a JEOL JSM-7610F scanning electron microscope. Samples were subjected to Pt sputtering for 100 s prior to observation. X-ray photoelectron spectroscopy (XPS) spectra were were performed on a British VG Scientific ESCALAB 250 system.

2.4. Photocatalytic experimental

The photocatalytic experiments were carried out in a 35 mL Pyrex reactor. The reactor was closed using rubber septum's. In a typical photocatalytic reaction, polymers powder (5 mg) was dispersed in 10 mL of the mixture of water/methanol/triethylamine (TEA) (1/1/1). The suspension was purged with argon for 5 min to remove dissolved air. After that, the samples were irradiated by a 350 W Xenon lamp equipped with a cut-off filter (1000 W/m^2, λ: 380–780 nm), and the reaction temperature was kept fixed at 25 °C using flowing cooling water. The formation of hydrogen was confirmed by injecting 0.5 μL of the reactor headspace gas in a Shimazhu gas chromatograph (GC2014) operating at isothermal conditions using a semi-capillary column equipped with a thermal conductivity detector.

2.5. Quantum efficiency measurements

In the AQY experiments, the catalyst solution was prepared by dispersing polymers powder (5 mg) in 10 mL of the mixture of water/methanol/triethylamine (TEA) (1/1/1). The suspension was illuminated with a 300 W Xe lamp with different bandpass filters (420, 460 and 500 nm). The formation of hydrogen was quantified using a Shimazhu gas chromatograph (GC2014) operating at isothermal conditions using a semi-capillary column equipped with a thermal conductivity detector. The AQY was calculated as follow:

AQY = [(Number of evolved hydrogen molecules × 2) / Number of incident photons] × 100%

$$AQY = \frac{N_e}{N_p} \times 100\% = \frac{2 \times M \times N_A}{\frac{E_{total}}{E_{photon}}} \times 100\%$$

$$= \frac{2M \times N_A}{\frac{S \times P \times t}{h \times \frac{c}{\lambda}}} \times 100\% = \frac{2 \times M \times N_A \times h \times c}{S \times P \times t \times \lambda} \times 100\%$$

where M is the amount of H_2 molecules (mol), NA is Avogadro constant (6.022×10^{23}/mol), h is the Planck constant (6.626×10^{-34} J·s), c is the speed of light (3×10^8 m/s), S is the irradiation area (cm^2), P is the intensity of irradiation light (W/cm^2), t is the photoreaction time (s), λ is the wavelength of the monochromatic light (m).

2.6. Photocatalytic stability test

The photocatalytic stability test was carried out as a similar procedure in the photocatalytic experiments section. The polymers powder (5 mg) was dispersed in 10 mL of the mixture of water/methanol/triethylamine (TEA) (1/1/1) and was tested over 6 h under visible light illumination (λ = 380–780 nm, Xe light source), the solution was then evaporated under vacuum at 70° C, then repeated for each cycle.

3. Results and discussion

To accomplish this work, we choose two building blocks featuring promising properties. The triphenyl triazine monomer as the triazine nitrogen atom, with its free electron pair and can act as the active site for an interface redox reaction, while the pyrene monomer is a fundamental polycyclic aromatic system that can undergo stacking by π–π interactions. Py-TPT-CMP and TPT-TPT-CMP were synthesized through Pd-catalyzed Suzuki coupling polymerization from 2,4,6-tris(4-(4,5-dimethyl-1,3,2-dioxaborolan-2-yl)phenyl)-1,3,5-triazine with 1,3,6,8-tetrabromopyrene and 2,4,6-tris(4-bromophenyl)-1,3,5-triazine, respectively (Scheme 1). Sulfur-doped CMPs were prepared by a thermal treatment of triazine-based CMPs with three concentrations (10, 20, and 30% wt) of sulfur and are denoted as Py-TPT-CMP-S_x and TPT-TPT-CMP-S_x (x = 10, 20, and 30) (Scheme 1). All synthetic procedures and routes are included in the Supplementary Information (Scheme S4–S7). The synthesized polymers are insoluble in common organic solvents due to their rigid backbone and the cross-linking networks. Their chemical structures were characterized with Fourier transform infrared (FT-IR) spectra, solid-state ^{13}C NMR spectra, and X-ray photoelectron spectroscopy (XPS). The FTIR spectra for all materials (Fig. 1a, b) show a characteristic vibration peak of the triazine ring unit at 815 cm^{-1}, whilst peaks located between 1200 and 1610 cm^{-1} originate from the stretching vibration modes of C—N and C═N heterocycle [66]. However, no peaks were ascribed to the bonding of sulfur with other elements because of the low amount of sulfur [54]. But the peaks located in the region from 1200 to 1610 cm^{-1} which are assignable to the stretching vibration modes of C-N and C═N heterocycles decrease with the sulfur doping, and this revealed that the introduced sulfur may replace the N atoms in the triazine units [67]. The solid state ^{13}C NMR spectra were conducted to explore the chemical environment of the C element for polymers and their monomer (Fig. 1c). The ^{13}C NMR spectra of the building block TPT-3Bpin featured characteristic peaks at 173 ppm of C═N. After polycondensations, the solid state ^{13}C NMR spectra of Py-TPT-CMP and TPT-TPT-CMP were characterized by the appearance of single main peaks at around 178 ppm for of the triazine core, in addition three peaks at 128.56, 136.51, and 145.46 ppm corresponding to the resonances of the aromatic carbon. However, for sulfur-doped CMPs, no peaks were ascribed to the bonding of sulfur with other elements (Fig. S5). We further characterize the porosity of the polymers using N_2 adsorption/desorption experiments at 77 K. The adsorption/desorption curves of the polymers (Figs. 1e and S6) were type I isotherms, this indicates that the synthesized polymers possess microporous structures. The apparent Brunauer–Emmett–Teller (BET) surface area (Figs. 1d, S6 and Table S1) are 953, 720, 588, 546, 510, and 405 $m^2 g^{-1}$, for Py-TPT-CMP, Py-TPT-CMP-S_{10}, Py-TPT-CMP-S_{20}, TPT-TPT-CMP, TPT-TPT-CMP-S_{10}, and TPT-TPT-CMP-S_{20}, respectively. Both layer structures and high BET surface areas are favorable for improving the dispersity of catalysts and their contact with reactants and thereby are profitable to the hydrogen production. The pore size distribution diagrams of the synthesized polymers have been constructed using the non-local density functional theory (NLDFT), the results (Figs. 1e, S6 and Table S1) show that the pore size of our polymers in the range from 1.23 to 1.86 nm, suggesting that our synthesized polymers are micropores polymers. X-ray photoelectron spectroscopy (XPS) was conducted to further identify the chemical composition of our CMPs. Figs. 2 and S7 show the high-resolution X-ray photoelectron spectra for all elements, where the high-resolution C1s spectra of the Py-TPT-CMP and TPT-TPT-CMP show two peaks at 284.4 and 285.8 eV, which are attributed to C—C═C and N—C═N, respectively, and an additional strong peak at 385.1 eV, corresponding to S—C═N, for Py-TPT-CMP-S_x and TPT-TPT-CMP-S_x reveals that an sulfur atom is indeed covalently bound to the backbone [54].

Furthermore, the of N—C═N peaks have been dramatically to the low bending energy direction with increasing the sulfur ratio, which should be attributed to the replaces of N in the triazine ring to form C—S bonds. The high-resolution spectra of N 1 s shows that the binding energy of the sp^2-hybridized aromatic N bonded to carbon atoms of Py-TPT-CMP and TPT-TPT-CMP at 399.0 eV. In particular, after sulfur doping, the new two peaks have been observed at binding energies of 398.6 and 399.1 eV, indicating two kinds of N arise from the incorporation of sulfur into the triazine ring of Py-TPT-CMP-S_x and TPT-TPT-CMP-S_x (Figs. 2 and S7). As the ratio of sulfur increased, the intensity ratio of N-C-N peaks have been dramatically decreased and the intensity ratio of N-C-S peaks have been increased, which should be attributed to the S-C bond formation in triazine rings. The high-resolution spectra of S2p (Figs. 2 and S7), a signal deriving from sulfur at 264.2 and 266.2 eV ($2p_{3/2}$ and $2p_{1/2}$) is clearly found in the sulfur-doped triazine-based CMPs, whereas it is not observed in Py-TPT-CMP and TPT-TPT-CMP, which is also an evidence for replaces N in triazine ring to form C–S bonds [54,68]. Furthermore, it can be clearly seen that, the S2p peaks obviously shifted to the low bending energy direction with increasing the sulfur ratio, clearly revealing the enhancement of S-C bonds.

The morphology of triazine-based CMPs were investigated by field-

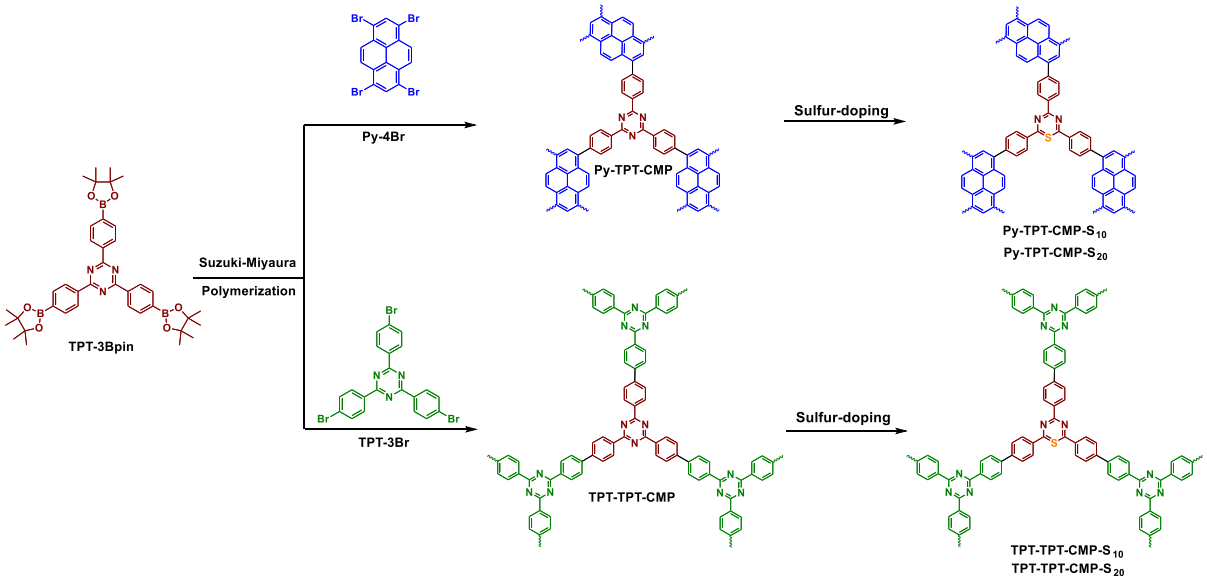

Scheme 1. Synthesis of triazine-based CMPs and sulfur-doped triazine-based CMPs.

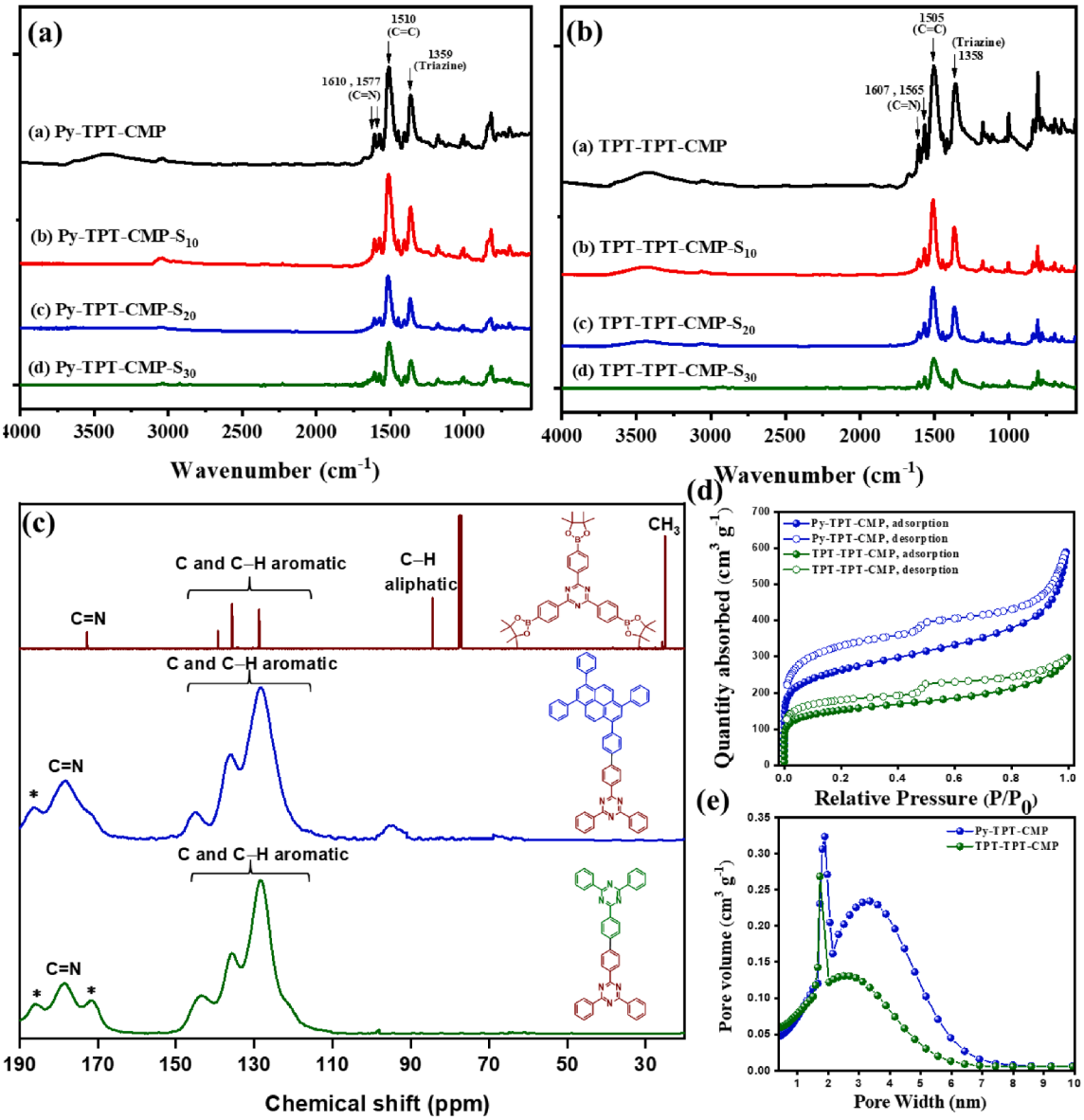

Fig. 1. (a, b) FT-IR spectra, (c) Solid-stated ^{13}C NMR spectra, (d) Nitrogen adsorption (filled symbols)/desorption (empty symbols) isotherms for the polymer collected at 77 K, and (e) Pore size distribution curves calculated by NLDFT.

emission scanning electron microscopy (FE-SEM) and transmission electron microscopy (TEM). As revealed from the SEM and TEM images shown in Fig. 3, triazine-based CMPs appear to have a porosity structure. In comparison to pure CMPs, the sulfur-doped CMPs sample (Figs. S8 and S9) have an aggregated structure with many smaller particles. Furthermore, the thermal stability of the synthesized polymers was revealed by TGA (Fig. S10). The TGA experiments were performed using a constant flow of nitrogen gas at range 100–800 °C by heating the samples at a rate of 10 °C min^{-1}. Py-TPT-CMP and TPT-TPT-CMP can remain stable up to 450 and 513 °C, respectively, while Py-TPT-CMP-S_{10}, Py-TPT-CMP-S_{20}, TPT-TPT-CMP-S_{10}, and TPT-TPT-CMP-S_{20} can remain stable up to 609, 560, 585, and 575 °C, respectively (Table S4). This result demonstrates that the sulfur-doped polymers present high thermal stability, which is necessary for the photocatalytic process [69].

UV–vis diffuse reflectance spectra of the triazine-based CMPs and their monomers are shown in Fig. 4a and S11-13. The absorption spectra of the polymers and their monomers were measured in dimethylformamide (DMF) at room temperature. As shown in Fig. S13, the UV visible absorption spectra of three monomers show an absorption band in the UV region, indicating that they cannot absorb visible light. The TPT-TPT-CMP shows light absorption from UV to visible light with an absorption edge of 410 nm, which can be assigned to the intrinsic band gap (3.01 eV) as shown in Fig. 4a. After doping with sulfur, the visible-light absorption intensities of TPT-TPT-CMP-S_x are significantly enhanced, and the red shifts are also observed on the sulfur-doped CMPs. The Py-TPT-CMP shows better visible-light absorption than TPT-TPT-CMP. Likewise, the absorption commences improve along with increase of sulfur doping amount in the Py-TPT-CMP-S_x. The observed shift of the absorption for the CMP-S_x materials indicates that the sulfur-doped strategy is indeed effective in extending the optical response of TPT-TPT-CMP and Py-TPT-CMP in the visible-light region. The optical bandgaps estimated from the Tauc plot as shown in Fig. S14 and Table 1. The highest occupied molecular orbital (HOMO) energy levels of the prepared polymers were determined using a photoelectron spectrometer and the lowest unoccupied molecular orbital (LUMO) level can be obtained by subtracting the Eg from HOMO energy level. As shown in Fig. 4b, the lowest unoccupied molecular orbital (LUMO) levels of the polymers higher than the potential of water reduction ranging from −2.40 to −3.55 eV are all able to drive the hydrogen evolution reaction (Table 1).

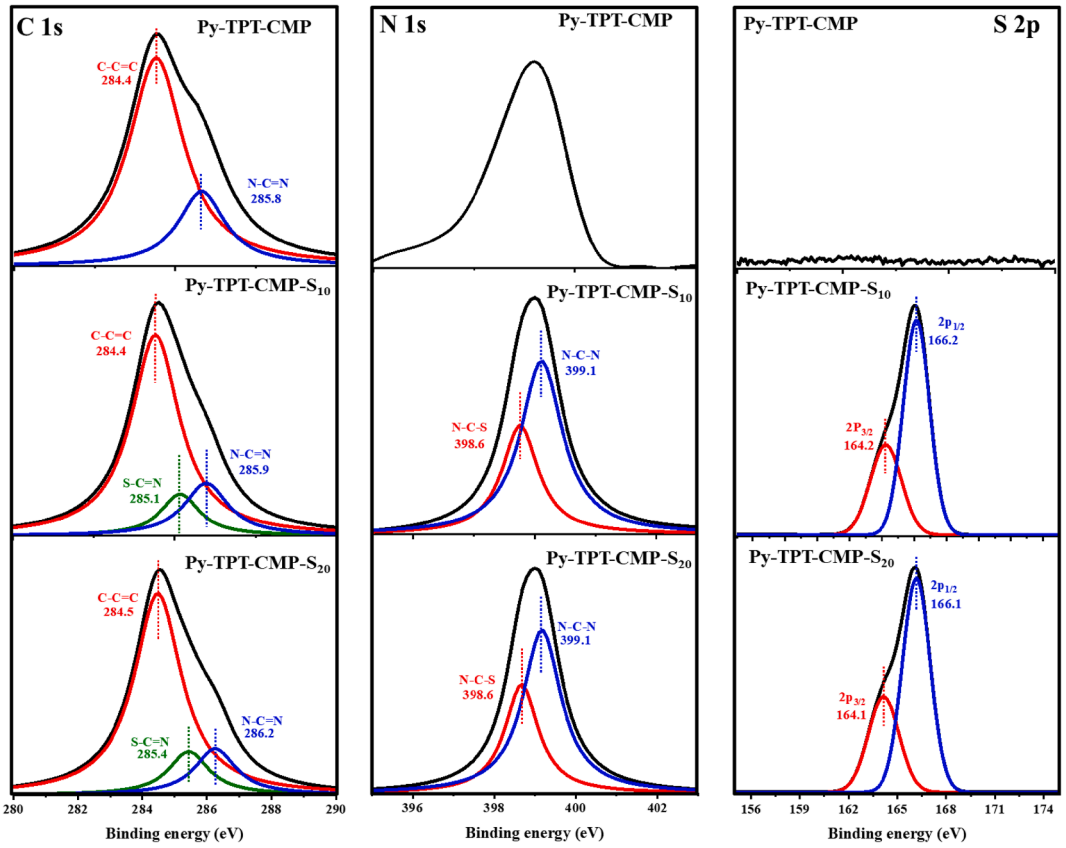

Fig. 2. High resolution XPS spectra of the C1s, N1s and S2p peaks for Py-TPT-CMP, Py-TPT-CMP S_{10}, and Py-TPT-CMP S_{20}.

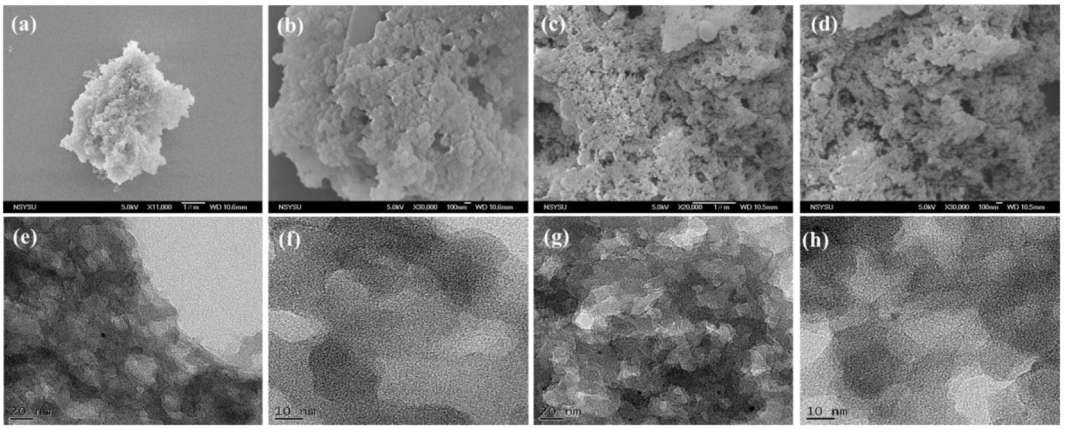

Fig. 3. (a, b) SEM images of TPT-TPT-CMP, (c, d) SEM images of Py-TPT-CMP, (e, f) TEM images of TPT-TPT-CMP, and (g, h) TEM images of Py-TPT-CMP.

To further explore the influence of doping of triazine-based CMPs with sulfur on photocatalytic efficiency and stability, we performed a series of photocatalytic activity tests of triazine-based CMPs and sulfur-doped CMPs. The photocatalytic activities for hydrogen evolution using triazine-based CMPs and sulfur-doped CMPs, and their monomers suspended in a solvent mixture consisting of equal volumes of water, methanol, and triethylamine (TEA) are evaluated at ambient temperature under visible-light irradiation, and the hydrogen evolution rate (HER) was analyzed using gas chromatography. TEA acts as a sacrifice electron donor (SED) and methanol is used to reduce phase segregation between TEA and water [70,71]. While methanol is known to also act as a SED in some cases [62,72], no activity has been observed in our case. All polymers were tested as synthesized and no additional cocatalysts were added. Triethanolamine (TEOA), TEA and ascorbic acid have been used as a SED. As seen in the Figs. S16 and S17, the HER produced by the photochemical reaction is the highest with TEA as SED. The monomer units did not show photocatalytic activities under the same conditions as shown in Figs. S18 and S19, thus illustrating that polymers are more active because of the enhanced optical absorption resulting from the extended delocalization. As shown in Figs. 4c, S23 and Table S6, the triazine-based CMPs show high photocatalytic performance and a hydrogen evolution rate of 108.11 and 116.50 μmol h^{-1} under visible-light for Py-TPT-CMP and TPT-TPT-CMP, respectively, indicating the important role of both the porosity and triazine unit. As shown in Fig. 4d, TPT-CMP has a high catalytic efficiency but a low catalytic stability. In practical applications, an effective photocatalyst should maintain its activity over a long period of time. Recycling experiments were therefore conducted (Figs. 4d and S20), in which the sulfur-doped

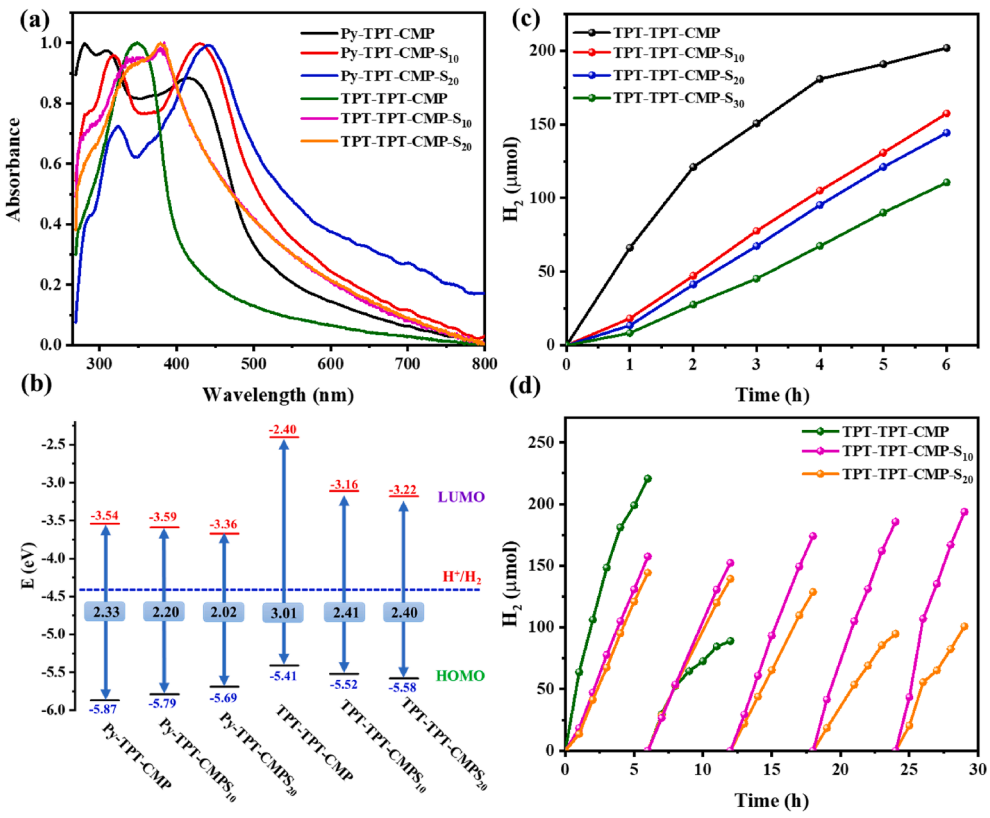

Fig. 4. (a) UV–vis diffuse absorption spectra of the polymers, (b) Electronic band structure of polymers, where the blue line represents the redox potential of H^+/H_2, (c) Hydrogen evolution under visible-light irradiation (λ: *380–780* nm) using TPT-based polymers, (d) Stability and reusability test using TPT-based polymers as a photocatalyst under visible-light irradiation. (For interpretation of the references to colour in this figure legend, the reader is referred to the web version of this article.)

Table 1
Photophysical properties and hydrogen evolution rate of the polymers.

Polymer	HOMO/ LUMO [eV][a,b]	Bandgap [eV][c]	HER [µmol h^{-1}][d]	AQY [%][e]		
				420 nm	460 nm	500 nm
PY-TPT-CMP	−5.87/-3.54	2.33	108.11	41.9	41.8	8.66
PY-TPT-$CMPS_{10}$	−5.79/-3.59	2.20	23.97	6.58	4.42	1.57
PY-TPT-$CMPS_{20}$	−5.69/-3.67	2.02	20.66	3.09	2.77	0.93
TPT-TPT-CMP	−5.41/-2.40	3.01	116.50	32.38	30.96	6.72
TPT-TPT-$CMPS_{10}$	−5.52/-3.11	2.41	53.76	10.91	7.06	1.52
TPT-TPT-$CMPS_{20}$	−5.58/-3.18	2.40	47.39	10.31	4.38	1.02

[a]HOMO determined by photoelectron spectrometry; [b]LUMO derived by extracting the $E_{HOMO} - E_g$; [c]Calculated from the absorption onsets; [d]Conditions; 10 mg polymer in 20 mL of the mixture of water/methanol/TEA (1/1/1), measured by 350 W Xenon light (AM 1.5, λ: 380–780 nm, 1000 W m^{-2}); [e]The AQY is measured at 420, 460, and 500 nm.

CMPs represents a good stability as photocatalyst which can keep the HER in more than five cycles, each cycle is 6 h without loss in the photocatalytic efficiency. In addition, we performed the stability again over than 100 h for Py-TPT-CMP-S_{10} and TPT-TPT-CMP-S_{10} as shown in Figs. S21 and S22, the polymers showed good stability over 80 h without a loss in photocatalytic efficiency. The results indicate that the doping of the sulfur atom into triazine ring has a significantly favorable impact on photocatalytic stability. However, with further increasing the ratio of sulfur, the photocatalytic efficiency has been decreased, this may be due to the decrease in the surface area as shown in Figs. 4c, S23 and Table S1. It is interesting to note that the photocatalytic performance of TPT-TPT-CMP-S_{10} improves with re-use and its efficacy in achieving pristine TPT-TPT-CMP performance (Fig. 4d). The higher stability of sulfur-doped triazine-based CMPs compared to that of triazine-based CMPs, because when replacing a nitrogen atom in a triazine ring, a sulfur atom must lose one electron to avoid the formation of unstable radical sites. So, sulfur-doped triazine rings were assumed to have a positive charge [73]. Therefore, when the excited electrons were captured by sulfur vacancy, the recombination of electrons and holes was suppressed. Also, localized charges around the substitution site and sulfur vacancy will promote the rapid migration of photogenerated carriers to the surface, consequently enhancing photocatalytic stability.

The generation of photoinduced electron-hole pairs, as well as separation and migration, is considered to be the basic process of photocatalytic reactions. Photoluminescence (PL) was used to measure the performance of charge carrier separation, transfer, and trapping. Hence, the lower intensity of PL is the higher charge separation [74]. The PL emission spectra of the polymers are shown in Fig. 5a. TPT-TPT-CMP and Py-TPT-CMP showed an increase in the PL peak intensity, indicating that the recombination of the charge carrier induced by a photocatalyst is high and this leads to a decrease in photostability of the catalyst. TPT-TPT-CMP-S_x and Py-TPT-CMP-S_x compared to TPT-TPT-CMP and Py-TPT-CMP, exhibited a dramatic decrease in the PL peak intensity, indicating that the recombination of the photoinduced charge carrier is quenched greatly after sulfur doping. This is because minor S dopants can behave as trapping sites to avoid the recombination of charge carries [75,76]. We observe that with increasing S-doping concentration, the PL intensity is decreasing, which is consistent with the PL study of S-doped nanowires [77,78]. Based on these results, it is hypothesized that the high photocatalytic stability of H_2 evolution is the consequence of S-doping, which is a significant factor in promoting the separation of photogenerated electron-hole pairs. Photocurrent of the polymers are studied during the on–off cycles with intermittent exposure of visible-light excitation (Figs. 5b and S24). Clearly, triazine-based CMPs show an improvement in photocurrent intensity relative to sulfur-doped triazine-based CMPs. This photocurrent result corroborates the

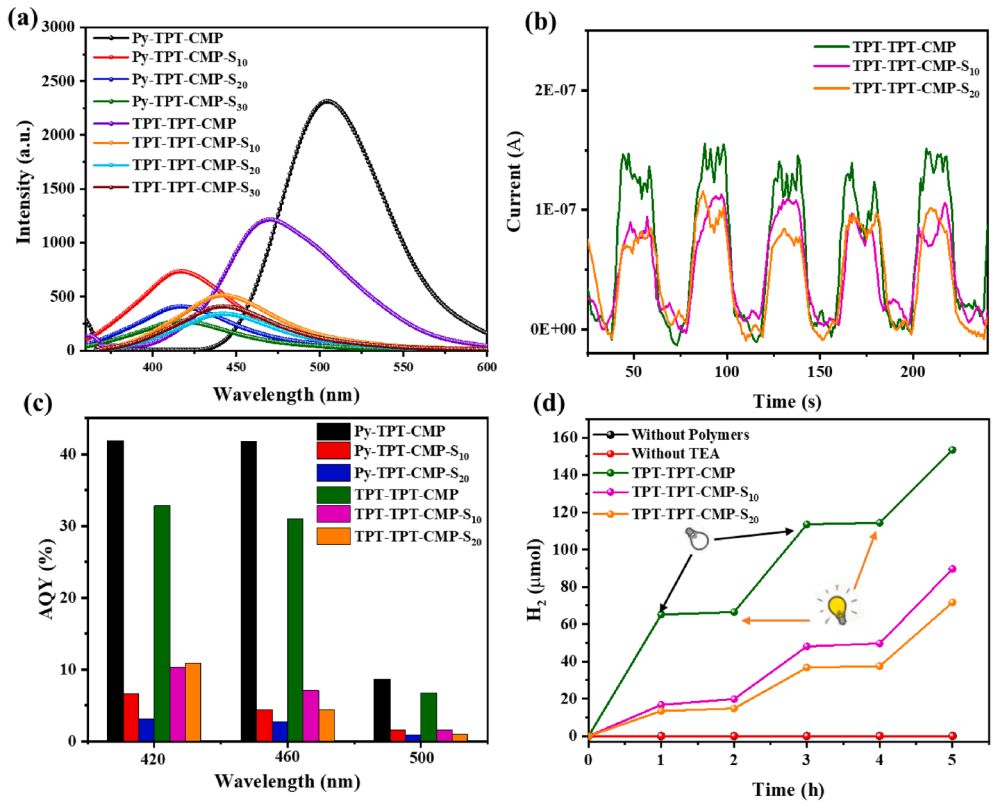

Fig. 5. (a) PL spectra of the polymers, (b) Photocurrent responses of TPT-based CMPs under visible light irradiation (LED lamp, λ > 420 nm), (c) Wavelength dependence of AQY on H_2 evolution of polymers, and (d) Control experiment of TPT-based polymers.

results from the photocatalytic performance. However, when the photocurrent carried out for a long time as shown in Fig. S25, the photocurrent of TPT-TPT-CMP-S_{10} persists for a long time (12 h) without reducing the current intensity, whereas the TPT-TPT-CMP was shown to reduce the current intensity with the time. In order to understand the relationship between sulfur doping and charge transfer efficiency in TPT-CMP, density-functional-theory (DFT) calculation was performed as shown in Figs. S26–29. The results showed that the introduction of sulfur could cause the rearrangement of the band structure in TPT-CMP, thus improving surface charge transfer efficiency. Figs. S30–S33 shown the effect of different amounts of sacrifice electron donor (TEA) on the H_2 evolution. We did not observe any significant effect on the rate of hydrogen evolution as the SED concentration increased. The effect of the photocatalyst amount on photocatalytic performance was investigated (Figs. S34 and S35). The hydrogen evolution performance is proportional to the mass of the catalysts used in the reaction. Different amounts of polymers (1.0, 3.0, and 5.0 mg) were used in 10 mL of the H_2O/MeOH/TEA mixed solvent, we observed that as the amount of photocatalyst increased, the photocatalytic efficiency increased (Figs. S34 and S35). As well as, we studied the effect of increasing the amount of photocatalyst using the same concentration of 0.5 mg/ml (2.5 mg/5mL, 5 mg/10 mL, and 10 mg/20 mL) (Fig. S36). We found that the photocatalytic efficiency improved with the rise in photocatalyst amounts, reaching 116.5 and 108.1 μmol h^{-1} for TPT-TPT-CMP and Py-TPT-CMP, respectively, as summarized in Table S5. Where this is so important at using in large scale in practical applications.

The apparent quantum yield (AQY) for the hydrogen evolution was measured under the illumination of a 300 W Xe lamp with different bandpass filters (420, 460 and 500 nm) (Fig. 5c). Our materials triazine-based CMPs exhibited significantly high AQY values, particularly for Py-TPT-CMP and TPT-TPT-CMP which exhibit AQY of 41.9 and 32.38, respectively at wavelengths = 420 nm as summarized in Table 1. The AQY of Py-TPT-CMP and TPT-TPT-CMP are the highest reported values for the triazine-based polymers to date (Fig. 6). Therefore, we measured the AQY at a different light intensity to confirm the results as shown in Fig. S37. This illustrates the importance of the higher surface area, which can absorb a large amount of the photons, as far as possible. We believe triazine has an enormous role to play in raising AQY, where high AQY was reported in several triazine-based polymer works. Jin et al. reported triazine with carbazole and benzothiadiazole with AQY = 22.8% [68], Cooper et al. reported triazine with benzonitrile with AQY = 15.9% [79], Li et al. reported triazine with thiophene and benzothiadiazole with AQY = 7.3% [80], and Wang et al. reported g-C_3N_4 with AQY about 11.97% at 400 nm [81]. Also, sulfur-doped TPT-based CMPs exhibit a higher AQY compared with other many organic semiconductors. The control experiments revealed that the kinetic curve of the photocatalytic process promptly decreased under light-off conditions and increased again under light-on conditions, conforming that our system undergoes a photocatalytic reaction (Figs. 5d and S38). As well as, the blank experiment by exposing the above H_2O/MeOH/TEA mixed solvents without the presence of any polymer catalysts to the xenon lamp didn't afford any hydrogen. Moreover, there is no hydrogen produce when the system was illuminated in the absence of TEA, which means here methanol has no activity as SED.

The FT-IR and XPS spectra of the polymers were recorded before and after the photocatalytic reaction (Figs. 7, 8, S39–42), which proves no change in the strcture of the prepared photocatalyst. In addition, the HRTEM images showed that our materials still have a porous structure after the photocatalytic reaction.

4. Photocatalytic mechanism

The photocatalytic activities for hydrogen evolution using triazine-based CMPs and sulfur-doped CMPs suspended in a solvent mixture consisting of equal volumes of water, methanol, and TEA are evaluated under visible-light irradiation. The mechanism of the excellent

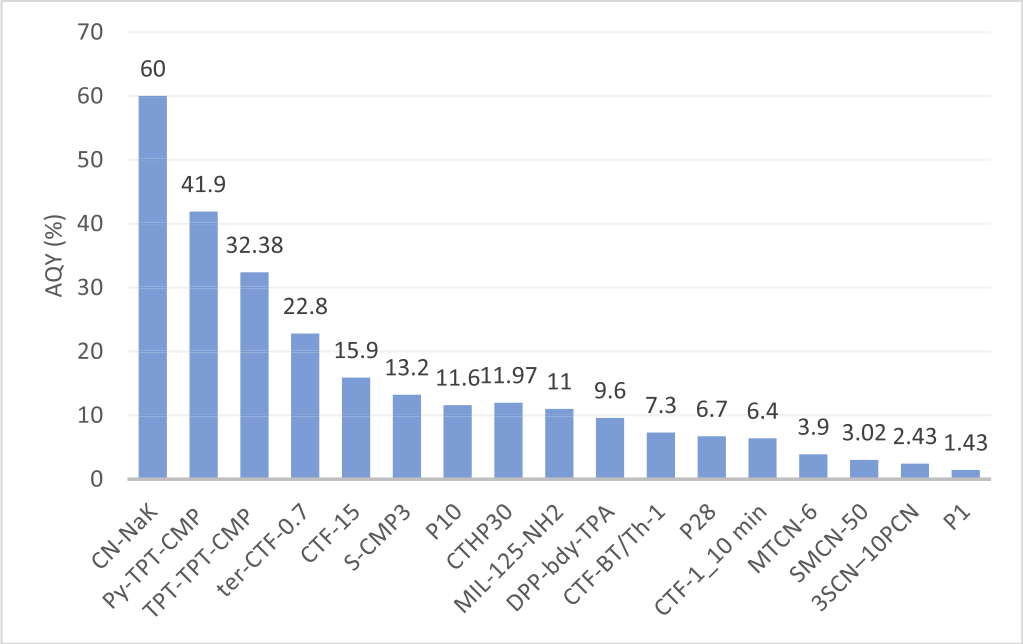

Fig. 6. Comparison of AQY measurements of H_2 under 420 nm of conjugated porous polymers with the highest reported AQY for g.C_3N_4.

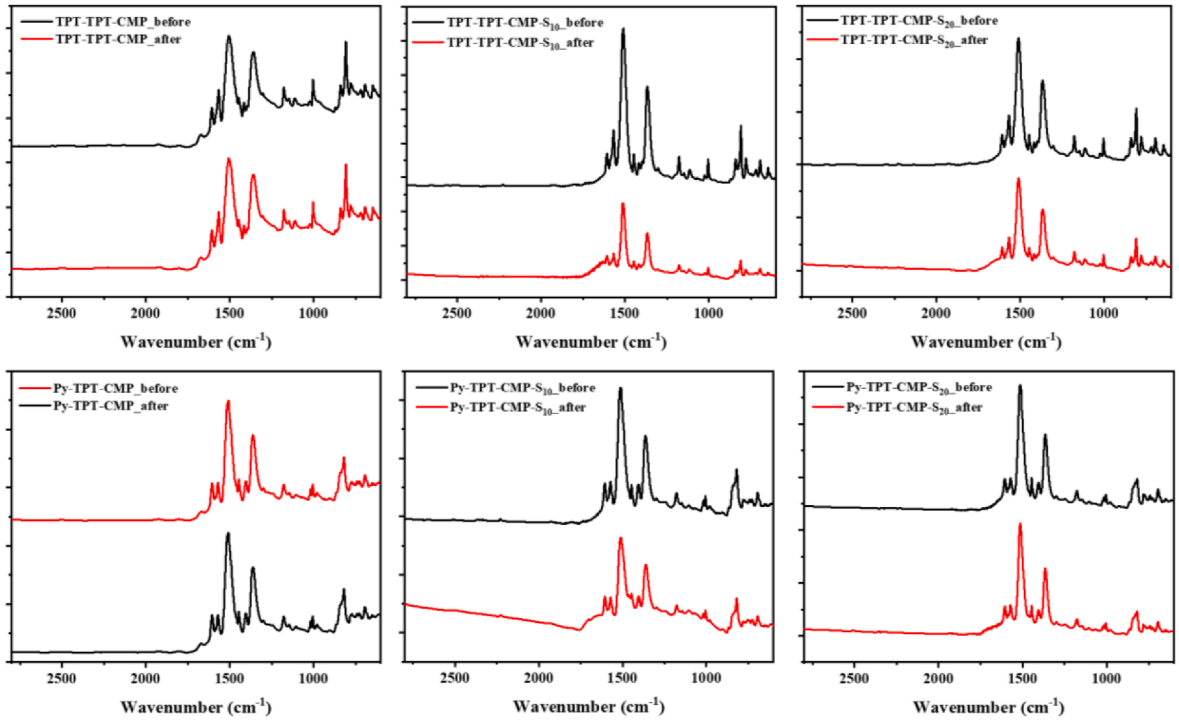

Fig. 7. (a) FT-IR spectra of TPT-based CMPs before and after photocatalytic reaction.

photocatalytic activity and stability of our materials after the doped sulfur species (S) replaces the lattice nitrogen atoms and forms the C–S chemical bonds in the triazine ring has been proposed as shown in Fig. 9. When replacing a nitrogen atom in a triazine ring, a sulfur atom must lose one electron to avoid the formation of unstable radical sites. So, sulfur-doped triazine rings were assumed to have a positive charge. Therefore, when the excited electrons were captured by sulfur vacancy, the recombination of electrons and holes was suppressed. Also, localized charges around the substitution site and sulfur vacancy will promote the rapid migration of photogenerated carriers to the surface, consequently enhancing photocatalytic stability. In addition, the above characterization and the experimental results, indicate that the substitution of lattice nitrogen by sulfur atoms can form a narrow band gap of TPT-CMP, and then enhance the light absorption in the visible region. As shown in UV – vis spectra, the absorption are gradually red-shifted with increasing content of sulfur. New doping-induced energy bands form in the top of the HOMO as the amount of doped sulfur atoms is adequate as shown in Fig. 9, the band gap for TPT-CMP becomes narrower. When the system is irradiated with visible light, electrons are excited from the HOMO and new HOMO level induced by sulfur doping to the LUMO of TPT-CMP.

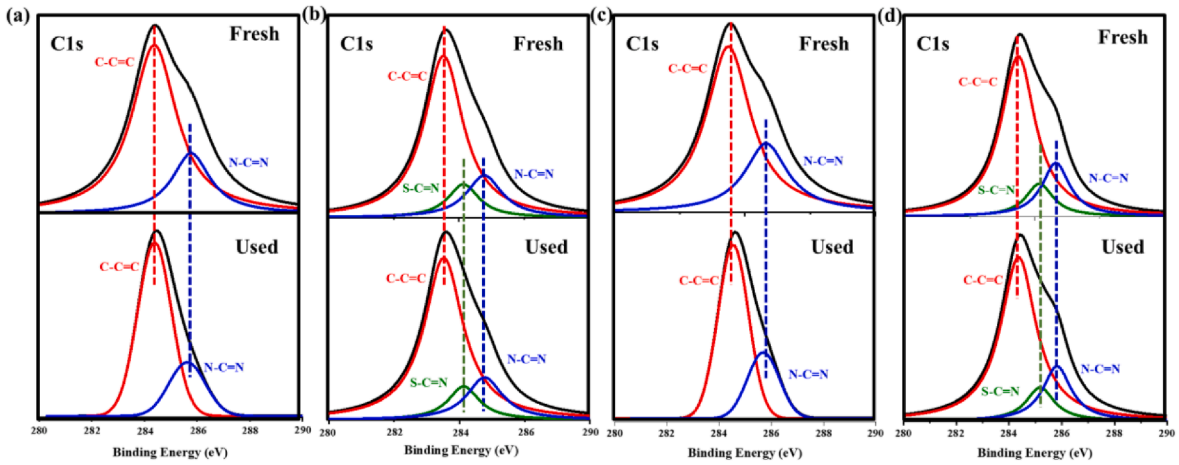

Fig. 8. High-resolution XPS spectra of the C1s peaks before and after photocatalytic reaction for (a) Py-TPT-CMP, (b) Py-TPT-CMP S_{10}, (c) TPT-TPT-CMP, and (d) TPT-TPT-CMP S_{10}.

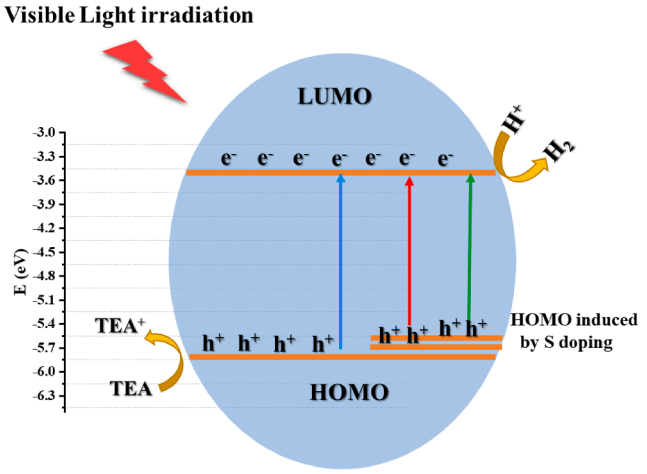

Fig. 9. The schematic diagram of photocatalytic mechanism over sulfur-doped TPT-CMP photocatalyst under visible light irradiation.

The maximum photocatalytic stability was achieved when the doping S content was 10%, as this caused maximum separation of the photo-electric charge carriers, thus preventing charges recombination. As the sulfur doping content increases, the position of the newly generated bandgap structures increases and then acts as recombination centers for the electron-hole pairs, because the distance between the charges to recombine becomes shorter than the distance needed for charge separation between both electrons and holes, so the photocatalytic performance and stability decrease.

5. Conclusions

In summary, we reported the synthesis and characterization of two triazine-based conjugated micropores polymers photocatalysts at low temperature for photocatalytic hydrogen production from water under visible light. The triazine-based CMPs show excellent photocatalytic performance and a hydrogen evolution rate of 108.1 and 116.5 μmol h^{-1} under visible-light for Py-TPT-CMP and TPT-TPT-CMP, respectively. These performances surpass many other reported porous materials. Furthermore, our triazine-based CMP materials have interest apparent quantum yield (AQY) values particularly for Py-TPT-CMP and TPT-TPT-CMP which exhibit AQY of 41.9% and 32.38%, respectively at 420 nm. The sulfur-doped CMPs photocatalysts were fabricated for enhancing their photocatalytic stability. The result indicates that the sulfur-doped CMPs represent excellent stability as photocatalysts which can keep the hydrogen production for a long period of time without loss in the photocatalytic efficiency.

Declaration of Competing Interest

The authors declare that they have no known competing financial interests or personal relationships that could have appeared to influence the work reported in this paper.

Acknowledgements

The authors gratefully acknowledge the financial support of the Ministry of Science and Technology of Taiwan (MOST 110-2636-E-007-020, MOST 110-2622-8-007-015, and MOST 108-2218-E-110-013-MY3), and also thank the National Center for High-Performance Computing of Taiwan for providing the computing time. The authors appreciate the Precision Instrument Support Center of National Tsing Hua University in providing the analysis and measurement facilities.

Appendix A. Supplementary data

Supplementary data to this article can be found online at https://doi.org/10.1016/j.cej.2021.129825.

References

[1] J. Jayakumar, H.H. Chou, Recent advances in visible-light-driven hydrogen evolution from water using polymer photocatalysts, ChemCatChem 12 (2020) 689–704.
[2] J. Huang, X. Li, X. Jin, L. Wang, Y. Deng, F. Su, P.K. Wong, L. Ye, High-efficiency and stable photocatalytic hydrogen evolution of rhenium sulfide co-catalyst on Zn 0.3 Cd 0.7 S, Mater. Adv. 1 (2020) 363–370.
[3] C. Jiang, L. Zhang, F. Gao, X. Huang, R. Lei, Y. Ye, J. Yuan, P. Liu, Promoting photocatalytic hydrogen production by a core–shell CdS@ MoO x photocatalyst connected by an S-Mo "bridge", Catal. Sci. Technol. 10 (2020) 1368–1375.
[4] H.A. Abbood, A. Alabadi, A.B. Al-Hawash, A.A. Abbood, K. Huang, Square CdS micro/nanosheets as efficient photo/piezo-bi-catalyst for hydrogen production, Cat. Lett. 150 (2020) 3059–3070.
[5] C. Liu, J. Li, L. Sun, Y. Zhou, C. Liu, H. Wang, P. Huo, C. Ma, Y. Yan, Visible-light driven photocatalyst of CdTe/CdS homologous heterojunction on N-rGO photocatalyst for efficient degradation of 2, 4-dichlorophenol, J. Taiwan Inst. Chem. Eng. 93 (2018) 603–615.
[6] H. Hieu, N. Nghia, N. Vuong, H. Van Bui, Omnidirectional Au-embedded ZnO/CdS core/shell nanorods for enhanced photoelectrochemical water-splitting efficiency, Chem. Commun. 56 (2020) 3975–3978.
[7] Q. Zhang, Y. Xiao, Y. Li, K. Zhao, H. Deng, Y. Lou, J. Chen, L. Cheng, NiS-Decorated ZnO/ZnS Nanorod Heterostructures for Enhanced Photocatalytic Hydrogen Production: Insight into the Role of NiS, Solar RRL 4 (2020) 1900568.

[8] L. Wang, L. Xie, W. Zhao, S. Liu, Q. Zhao, Oxygen-facilitated dynamic active-site generation on strained MoS2 during photo-catalytic hydrogen evolution, Chem. Eng. J. 405 (2021), 127028.

[9] Y. Wang, L. Shi, B. Qian, X. Huang, X. Sun, B. Wang, X.-M. Song, H. Huang, Y. Zhang, T. Ma, Regeneratable trinuclear iron-oxo cocatalyst for photocatalytic hydrogen evolution, Chem. Eng. J. 127551 (2020).

[10] L. Hu, Y. Li, X. Peng, W. Zheng, W. Xu, J. Zhu, L.Y.S. Lee, P.K. Chu, K.-Y. Wong, TiO2 film supported by vertically aligned gold nanorod superlattice array for enhanced photocatalytic hydrogen evolution, Chem. Eng. J. 127900 (2020).

[11] R.S. Sprick, C.M. Aitchison, E. Berardo, L. Turcani, L. Wilbraham, B.M. Alston, K. E. Jelfs, M.A. Zwijnenburg, A.I. Cooper, Maximising the hydrogen evolution activity in organic photocatalysts by co-polymerisation, J. Mater. Chem. A 6 (2018) 11994–12003.

[12] X. Feng, Y. Pi, Y. Song, C. Brzezinski, Z. Xu, Z. Li, W. Lin, Metal-organic frameworks significantly enhance photocatalytic hydrogen evolution and co2 reduction with earth-abundant copper photosensitizers, J. Am. Chem. Soc. 142 (2020) 690–695.

[13] R.S. Sprick, J.-X. Jiang, B. Bonillo, S. Ren, T. Ratvijitvech, P. Guiglion, M. A. Zwijnenburg, D.J. Adams, A.I. Cooper, Tunable organic photocatalysts for visible-light-driven hydrogen evolution, J. Am. Chem. Soc. 137 (2015) 3265–3270.

[14] W.-H. Wang, L.-Y. Ting, J. Jayakumar, C.-L. Chang, W.-C. Lin, C.-C. Chung, M. H. Elsayed, C.-Y. Lu, A.M. Elewa, H.-H. Chou, Design and synthesis of phenylphosphine oxide-based polymer photocatalysts for highly efficient visible-light-driven hydrogen evolution, Sustain. Energy Fuels 4 (2020) 5264–5270.

[15] Z. Cui, Y. Hu, Y. Zhang, Q. Han, Y. Wang, Y. Zhou, Z. Zou, A new triazine-based conjugated polymer from simple monomers with stable photocatalytic hydrogen evolution under visible light, Polymer 211 (2020), 123079.

[16] M. Luo, Q. Yang, W. Yang, J. Wang, F. He, K. Liu, H. Cao, H. Yan, Defects engineering leads to enhanced photocatalytic H_2 evolution on graphitic carbon nitride-covalent organic framework nanosheet composite, Small 16 (2020) 2001100.

[17] J.-H. Zhang, M.-J. Wei, Z.-W. Wei, M. Pan, C.-Y. Su, Ultrathin graphitic carbon nitride nanosheets for photocatalytic hydrogen evolution, ACS Appl. Nano Mater. 3 (2020) 1010–1018.

[18] K. Maeda, X. Wang, Y. Nishihara, D. Lu, M. Antonietti, K. Domen, Photocatalytic activities of graphitic carbon nitride powder for water reduction and oxidation under visible light, J. Phys. Chem. C 113 (2009) 4940–4947.

[19] M. Ismael, Y. Wu, D.H. Taffa, P. Bottke, M. Wark, Graphitic carbon nitride synthesized by simple pyrolysis: role of precursor in photocatalytic hydrogen production, New J. Chem. 43 (2019) 6909–6920.

[20] Y. Li, S. Zhu, Y. Xu, R. Ge, J. Qu, M. Zhu, Y. Liu, J.M. Cairney, R. Zheng, S. Li, J. Zhang, W. Li, FeS_2 bridging function to enhance charge transfer between MoS_2 and g–C_3N_4 for efficient hydrogen evolution reaction, Chem. Eng. J. 127804 (2020).

[21] C. Wan, L. Zhou, L. Sun, L. Xu, D.-G. Cheng, F. Chen, X. Zhan, Y. Yang, Boosting visible-light-driven hydrogen evolution from formic acid over AgPd/2D g-C3N4 nanosheets Mott-Schottky photocatalyst, Chem. Eng. J. 396 (2020), 125229.

[22] H. Cai, B. Wang, L. Xiong, G. Yang, L. Yuan, J. Bi, X. Yu, X. Zhang, S. Yang, S. Yang, Bridging effect of Co heteroatom between g-C3N4 and Pt NPs for enhanced photocatalytic hydrogen evolution, Chem. Eng. J. 394 (2020), 124964.

[23] M. Ismael, Y. Wu, M. Wark, Photocatalytic activity of ZrO_2 composites with graphitic carbon nitride for hydrogen production under visible light, New J. Chem. 43 (2019) 4455–4462.

[24] A. Mishra, A. Mehta, S. Basu, N.P. Shetti, K.R. Reddy, T.M. Aminabhavi, Graphitic carbon nitride (g–C_3N_4)–based metal-free photocatalysts for water splitting: a review, Carbon 149 (2019) 693–721.

[25] W.-J. Ong, L.-L. Tan, Y.H. Ng, S.-T. Yong, S.-P. Chai, Graphitic carbon nitride (g-C_3N_4)-based photocatalysts for artificial photosynthesis and environmental remediation: are we a step closer to achieving sustainability? Chem. Rev. 116 (2016) 7159–7329.

[26] C.B. Meier, R.S. Sprick, A. Monti, P. Guiglion, J.-S.-M. Lee, M.A. Zwijnenburg, A. I. Cooper, Structure-property relationships for covalent triazine-based frameworks: The effect of spacer length on photocatalytic hydrogen evolution from water, Polymer 126 (2017) 283–290.

[27] L.-Y. Ting, J. Jayakumar, C.-L. Chang, W.-C. Lin, M.H. Elsayed, H.-H. Chou, Effect of controlling the number of fused rings on polymer photocatalysts for visible-light-driven hydrogen evolution, J. Mater. Chem. A 7 (2019) 22924–22929.

[28] P.-J. Tseng, C.-L. Chang, Y.-H. Chan, L.-Y. Ting, P.-Y. Chen, C.-H. Liao, M.-L. Tsai, H.-H. Chou, Design and synthesis of cycloplatinated polymer dots as photocatalysts for visible-light-driven hydrogen evolution, ACS Catal. 8 (2018) 7766–7772.

[29] C.-L. Chang, W.-C. Lin, C.-Y. Jia, L.-Y. Ting, J. Jayakumar, M.H. Elsayed, Y.-Q. Yang, Y.-H. Chan, W.-S. Wang, C.-Y. Lu, P.-Y. Chen, H.-H. Chou, Low-toxic cycloplatinated polymer dots with rational design of acceptor co-monomers for enhanced photocatalytic efficiency and stability, Appl. Cat. B 268 (2020), 118436.

[30] Y. Bai, Z. Hu, J.X. Jiang, F. Huang, Hydrophilic conjugated materials for photocatalytic hydrogen evolution, Chem. Asian J. 15 (2020) 1780–1790.

[31] J. Wang, K. Feng, B. Chen, Z.-J. Li, Q.-Y. Meng, L.-P. Zhang, C.-H. Tung, L.-Z. Wu, Polymer-modified hydrophilic graphene: a promotor to photocatalytic hydrogen evolution for in situ formation of core@shell cobalt nanocomposites, J. Photochem. Photobiol. A chem. 331 (2016) 247–254.

[32] V.R. Battula, S. Kumar, D.K. Chauhan, S. Samanta, K. Kailasam, A true oxygen-linked heptazine based polymer for efficient hydrogen evolution, Appl. Cat. B 244 (2019) 313–319.

[33] K. Kailasam, J. Schmidt, H. Bildirir, G. Zhang, S. Blechert, X. Wang, A. Thomas, Room temperature synthesis of heptazine-based microporous polymer networks as photocatalysts for hydrogen evolution, Macromol. Rapid Commun. 34 (2013) 1008–1013.

[34] S. Mao, J.-W. Shi, G. Sun, Y. Zhang, X. Ji, Y. Lv, B. Wang, Y. Xu, Y. Cheng, Cu (II) decorated thiol-functionalized MOF as an efficient transfer medium of charge carriers promoting photocatalytic hydrogen evolution, Chem. Eng. J. 404 (2021), 126533.

[35] J. Rong, G. Zhu, W. Ryan Osterloh, Y. Fang, Z. Ou, F. Qiu, K.M. Kadish, In situ construction MoS2-Pt nanosheets on 3D MOF-derived S, N-doped carbon substrate for highly efficient alkaline hydrogen evolution reaction, Chem. Eng. J. (2020), 127556.

[36] A.F. EL-Mahdy, A.M. Elewa, S.W. Huang, H.H. Chou, S.W. Kuo, Dual-function fluorescent covalent organic frameworks: hcl sensing and photocatalytic h2 evolution from water, Adv. Optical Mater. 8 (2020) 2000641.

[37] P. Pachfule, A. Acharjya, J. Roeser, T. Langenhahn, M. Schwarze, R. Schomäcker, A. Thomas, J. Schmidt, Diacetylene functionalized covalent organic framework (COF) for photocatalytic hydrogen generation, J. Am. Chem. Soc. 140 (2018) 1423–1427.

[38] Y.-P. Zhang, H.-L. Tang, H. Dong, M.-Y. Gao, C.-C. Li, X.-J. Sun, J.-Z. Wei, Y. Qu, Z.-J. Li, F.-M. Zhang, Covalent-organic framework based Z-scheme heterostructured noble-metal-free photocatalysts for visible-light-driven hydrogen evolution, J. Mater. Chem. A 8 (2020) 4334–4340.

[39] A.M. Elewa, M.H. Elsayed, A.F.M. El-Mahdy, C.-L. Chang, L.-Y. Ting, W.-C. Lin, C.-Y. Lu, H.-H. Chou, Triptycene-based discontinuously-conjugated covalent organic polymer photocatalysts for visible-light-driven hydrogen evolution from water, Appl. Catal. B 285 (2021), 119802.

[40] X. Gao, C. Shu, C. Zhang, W. Ma, S.-B. Ren, F. Wang, Y. Chen, J.H. Zeng, J.-X. Jiang, Substituent effect of conjugated microporous polymers on the photocatalytic hydrogen evolution activity, J. Mater. Chem. A 8 (2020) 2404–2411.

[41] Y. Xu, N. Mao, S. Feng, C. Zhang, F. Wang, Y. Chen, J. Zeng, J.-X. Jiang, Perylene-containing conjugated microporous polymers for photocatalytic hydrogen evolution, Macromol. Chem. Phys. 218 (2017) 1700049.

[42] D. Wang, X. Li, L.-L. Zheng, L.-M. Qin, S. Li, P. Ye, Y. Li, J.-P. Zou, Size-controlled synthesis of CdS nanoparticles confined on covalent triazine-based frameworks for durable photocatalytic hydrogen evolution under visible light, Nanoscale 10 (2018) 19509–19516.

[43] J. Xie, S.A. Shevlin, Q. Ruan, S.J. Moniz, Y. Liu, X. Liu, Y. Li, C.C. Lau, Z.X. Guo, J. Tang, Efficient visible light-driven water oxidation and proton reduction by an ordered covalent triazine-based framework, Energy Environ. Sci. 11 (2018) 1617–1624.

[44] H.S. Jena, C. Krishnaraj, S. Parwaiz, F. Lecoeuvre, J. Schmidt, D. Pradhan, P. Van Der Voort, Illustrating the role of quaternary-N of BINOL covalent triazine-based frameworks in oxygen reduction and hydrogen evolution reactions, ACS Appl. Mater. Interfaces 12 (2020) 44689–44699.

[45] E. Jin, J. Li, K. Geng, Q. Jiang, H. Xu, Q. Xu, D. Jiang, Designed synthesis of stable light-emitting two-dimensional sp 2 carbon-conjugated covalent organic frameworks, Nat. Commun. 9 (2018) 1–10.

[46] L. Stegbauer, S. Zech, G. Savasci, T. Banerjee, F. Podjaski, K. Schwinghammer, C. Ochsenfeld, B.V. Lotsch, Photocatalysis: Tailor-Made Photoconductive Pyrene-Based Covalent Organic Frameworks for Visible-Light Driven Hydrogen Generation (Adv. Energy Mater. 24/2018), Adv. Energy Mater. 8 (2018) 1870107.

[47] Y. Zhao, W. Ma, Y. Xu, C. Zhang, Q. Wang, T. Yang, X. Gao, F. Wang, C. Yan, J.-X. Jiang, Effect of linking pattern of dibenzothiophene-S, S-dioxide-containing conjugated microporous polymers on the photocatalytic performance, Macromolecules 51 (2018) 9502–9508.

[48] M.G. Mohamed, M.H. Elsayed, A.M. Elewa, A.F. EL-Mahdy, C.-H. Yang, A. A. Mohammed, H.-H. Chou, S.-W. Kuo, Pyrene-containing conjugated organic microporous polymers for photocatalytic hydrogen evolution from water, Catal. Sci. Technol. 11 (2021) 2229–2241.

[49] Z.A. Lan, Y. Fang, Y. Zhang, X. Wang, Photocatalytic oxygen evolution from functional triazine-based polymers with tunable band structures, Angew. Chem. 130 (2018) 479–483.

[50] D. Kong, X. Han, J. Xie, Q. Ruan, C.D. Windle, S. Gadipelli, K. Shen, Z. Bai, Z. Guo, J. Tang, Tunable covalent triazine-based frameworks (CTF-0) for visible-light-driven hydrogen and oxygen generation from water splitting, ACS catal. 9 (2019) 7697–7707.

[51] T.N. Nguyen, S. Kampouri, B. Valizadeh, W. Luo, D. Ongari, O.M. Planes, A. Züttel, B. Smit, K.C. Stylianou, Photocatalytic hydrogen generation from a visible-light-responsive metal-organic framework system: stability versus activity of molybdenum sulfide cocatalysts, Appl. Mater. Interfaces 10 (2018) 30035–30039.

[52] M.Z. Rahman, M.G. Kibria, C.B. Mullins, Metal-free photocatalysts for hydrogen evolution, Chem. Soc. Rev. 49 (2020) 1887–1931.

[53] Y.J. Yuan, H.W. Lu, Z.T. Yu, Z.G. Zou, Noble-metal-free molybdenum disulfide cocatalyst for photocatalytic hydrogen production, ChemSusChem 8 (2015) 4113–4127.

[54] L. Li, W. Fang, P. Zhang, J. Bi, Y. He, J. Wang, W. Su, Sulfur-doped covalent triazine-based frameworks for enhanced photocatalytic hydrogen evolution from water under visible light, J Mater. Chem. A 4 (2016) 12402–12406.

[55] C. Wang, Y. Guo, Y. Yang, S. Chu, C. Zhou, Y. Wang, Z. Zou, Sulfur-doped polyimide photocatalyst with enhanced photocatalytic activity under visible light irradiation, ACS Appl. Mater. Interfaces 6 (2014) 4321–4328.

[56] H. Qin, W. Lv, J. Bai, Y. Zhou, Y. Wen, Q. He, J. Tang, L. Wang, Q. Zhou, Sulfur-doped porous graphitic carbon nitride heterojunction hybrids for enhanced photocatalytic H 2 evolution, J. Mater. Sci. 54 (2019) 4811–4820.

[57] Y. Okamoto, S. Ida, J. Hyodo, H. Hagiwara, T. Ishihara, Synthesis and photocatalytic activity of rhodium-doped calcium niobate nanosheets for hydrogen

production from a water/methanol system without cocatalyst loading, J. Am. Chem. Soc. 133 (2011) 18034–18037.
[58] M. Ismael, Enhanced photocatalytic hydrogen production and degradation of organic pollutants from Fe (III) doped TiO2 nanoparticles, J. Environ. Chem. Eng. 8 (2020), 103676.
[59] M. Ismael, Highly effective ruthenium-doped TiO_2 nanoparticles photocatalyst for visible-light-driven photocatalytic hydrogen production, New J. Chem. 43 (2019) 9596–9605.
[60] G. Zhang, M. Zhang, X. Ye, X. Qiu, S. Lin, X. Wang, Iodine modified carbon nitride semiconductors as visible light photocatalysts for hydrogen evolution, Adv. mater. 26 (2014) 805–809.
[61] R. Asahi, T. Morikawa, T. Ohwaki, K. Aoki, Y. Taga, Visible-light photocatalysis in nitrogen-doped titanium oxides, Science 293 (2001) 269–271.
[62] L. Ge, C. Han, X. Xiao, L. Guo, Y. Li, Enhanced visible light photocatalytic hydrogen evolution of sulfur-doped polymeric g-C_3N_4 photocatalysts, Mater. Res. Bull. 48 (2013) 3919–3925.
[63] D. Long, L. Wang, H. Cai, X. Rao, Y. Zhang, Sulfur doped carbon-rich gC 3 N 4 for enhanced photocatalytic H 2 evolution, Morphol. Crystall. Effect Cat. Lett. (2020) 1–10.
[64] A.F. El-Mahdy, C.H. Kuo, A. Alshehri, C. Young, Y. Yamauchi, J. Kim, S.W. Kuo, Strategic design of triphenylamine-and triphenyltriazine-based two-dimensional covalent organic frameworks for CO_2 uptake and energy storage, J. Mater. Chem. A 6 (2018) 19532–19541.
[65] A.F. El-Mahdy, C. Young, J. Kim, J. You, Y. Yamauchi, S.-W. Kuo, Hollow microspherical and microtubular [3+ 3] carbazole-based covalent organic frameworks and their gas and energy storage applications, ACS Appl. Mater. Interfaces 11 (2019) 9343–9354.
[66] Y. Li, S. Wang, W. Chang, L. Zhang, Z. Wu, S. Song, Y. Xing, Preparation and enhanced photocatalytic performance of sulfur doped terminal-methylated $gC_{3\ N}4$ nanosheets with extended visible-light response, J. Mater. Chem. A 7 (2019) 20640–20648.
[67] C. Feng, L. Tang, Y. Deng, J. Wang, Y. Liu, X. Ouyang, H. Yang, J. Yu, J. Wang, A novel sulfur-assisted annealing method of g-C_3N_4 nanosheet compensates for the loss of light absorption with further promoted charge transfer for photocatalytic production of H_2 and H_2O_2, Appl. Catal. B 281 (2021), 119539.
[68] L. Guo, Y. Niu, S. Razzaque, B. Tan, S. Jin, Design of D-A1–A2 Covalent Triazine Frameworks via Copolymerization for Photocatalytic Hydrogen Evolution, ACS Catal. 9 (2019) 9438–9445.
[69] Y. Chen, D. Yang, B. Shi, W. Dai, H. Ren, K. An, Z. Zhou, Z. Zhao, W. Wang, Z. Jiang, In situ construction of hydrazone-linked COF-based core–shell hetero-frameworks for enhanced photocatalytic hydrogen evolution, J. Mater. Chem. A 8 (2020) 7724–7732.
[70] M. Sachs, R.S. Sprick, D. Pearce, S.A. Hillman, A. Monti, A.A. Guilbert, N. J. Brownbill, S. Dimitrov, X. Shi, F. Blanc, Understanding structure-activity relationships in linear polymer photocatalysts for hydrogen evolution, Nat. commun. 9 (2018) 1–11.
[71] L. Li, W.-Y. Lo, Z. Cai, N. Zhang, L. Yu, Donor–acceptor porous conjugated polymers for photocatalytic hydrogen production: the importance of acceptor comonomer, Macromolecules 49 (2016) 6903–6909.
[72] X. Wang, K. Maeda, A. Thomas, K. Takanabe, G. Xin, J.M. Carlsson, K. Domen, M. Antonietti, A metal-free polymeric photocatalyst for hydrogen production from water under visible light, Nat. Mater. 8 (2009) 76–80.
[73] T.-J. Lin, C.-C. Chiu, Influence of nonmetal dopants on charge separation of graphitic carbon nitride by time-dependent density functional theory, Phys. Chem. Chem. Phys. 22 (2020) 647–657.
[74] S.B. Babar, N.L. Gavade, D.P. Bhopate, A.N. Kadam, S.B. Kokane, S.D. Sartale, A. Gophane, K.M. Garadkar, V.M. Bhuse, An efficient fabrication of ZnO–carbon nanocomposites with enhanced photocatalytic activity and superior photostability, J. Mater. Sci. Mater. Electron. 30 (2019) 1133–1147.
[75] Q. Guo, Y. Zhang, J. Qiu, G. Dong, Engineering the electronic structure and optical properties of gC 3 N 4 by non-metal ion doping, J. Mater. Chem. C 4 (2016) 6839–6847.
[76] H. Wang, Y. Bian, J. Hu, L. Dai, Highly crystalline sulfur-doped carbon nitride as photocatalyst for efficient visible-light hydrogen generation, Appl. Catal. B 238 (2018) 592–598.
[77] W. Zhang, S. Lehmann, K. Mergenthaler, J. Wallentin, M.T. Borgström, M.-E. Pistol, A. Yartsev, Carrier recombination dynamics in sulfur-doped InP nanowires, Nano Lett. 15 (2015) 7238–7244.
[78] J. Wallentin, K. Mergenthaler, M. Ek, L.R. Wallenberg, L. Samuelson, K. Deppert, M.-E. Pistol, M.T. Borgström, Probing the wurtzite conduction band structure using state filling in highly doped InP nanowires, Nano Lett. 11 (2011) 2286–2290.
[79] C.B. Meier, R. Clowes, E. Berardo, K.E. Jelfs, M.A. Zwijnenburg, R.S. Sprick, A. I. Cooper, Structurally diverse covalent triazine-based framework materials for photocatalytic hydrogen evolution from water, Chem. Mater. 31 (2019) 8830–8838.
[80] W. Huang, Q. He, Y. Hu, Y. Li, Molecular heterostructures of covalent triazine frameworks for enhanced photocatalytic hydrogen production, Angew. Chem. Int. Ed. 58 (2019) 8676–8680.
[81] C. Wu, G. Yu, Y. Yin, Y. Wang, L. Chen, Q. Han, J. Tang, B. Wang, Mesoporous polymeric cyanamide-triazole-heptazine photocatalysts for highly-efficient water splitting, Small 16 (2020) 2003162.